Proceedings of the DIS'2004, Štrbské Pleso, Slovakia

DIJET PRODUCTION IN DIS AND PHOTOPRODUCTION

MATTHEW LIGHTWOOD,
Weizmann Institute of Science
Rehovot 76100 , Israel
E-mail: lightwd@mail.desy.de

The dependence of dijet production on the virtuality of the exchanged photon, Q^2 has been studied in the range $0.0 < Q^2 < 2000$ GeV^2. The variable $x_\gamma^{\rm OBS}$ was used to enhance the sensitivity of the measurements to the photon structure. Detailed comparisons of the data to next-to-leading-order QCD predictions is given. The predictions are shown to generally underestimate the cross sections in regions where the effects of photon structure are expected.

1 Introduction

Interactions involving real or quasi-real photons ($Q^2 \approx 0$, where Q^2 is the virtuality of the photon) are well described by calculations that use a partonic structure for the photon [1,2]. However, in deep inelastic scattering (DIS), where Q^2 is large, the virtual photon is commonly treated as a point-like object and used as a probe of the partonic structure of nucleons [3,4,5]. In this paper, dijet production is investigated over a large range of incident photon virtualities, including photoproduction, DIS, and the transition region between them. Both the H1 [6,7] and ZEUS [8] collaborations have previously studied the transition between photoproduction and DIS by measuring inclusive jet and dijet cross sections in ep collisions.

Two processes contribute to the jet photoproduction cross section at leading order (LO) in quantum chromodynamics (QCD) direct, in which the photon couples as a point-like particle to quarks in the hard scatter; and resolved, in which the photon acts as a source of partons. Both processes can lead to two jets in the final state. The $x_\gamma^{\rm OBS}$ variable, which is the fraction of the photon momentum participating in the production of the dijet system, is used to separate the two processes since resolved (direct) processes dominate at low (high) $x_\gamma^{\rm OBS}$ values [9,10].

In this paper, the validity of fixed order calculations in describing dijet production is investigated. Cross sections differential with respect to Q^2, $E_T^{\rm jet1}$ and η^F, have been measured in photoproduction and DIS, where $E_T^{\rm jet1}$ is the E_T of the which has the highest transverse energy, and η^F is the pseudorapidity of the most forward jet. The ratio of low- to high-$x_\gamma^{\rm OBS}$ components is measured as a function of Q^2 in different regions of $\overline{E}_T^2$, where $\overline{E}_T^2$ is the square of the average transverse energy of the two jets with highest transverse energy. A more complete description of these results can be found in [11].

2 Cross section definition

The cross sections were measured in the range $0 < Q^2 < 2000$ GeV^2 and $0.2 < y < 0.55$. Jets were reconstructed with the $\mathrm{k_T}$ cluster algorithm [12] applied in the photon-proton centre-of-mass frame, in the longitudinally invariant inclusive mode [13]. At least two jets were required within the pseudorapidity range $-3 < \eta^{\mathrm{jet}} < 0$, satisfying $E_T^{\mathrm{jet1}} > 7.5$ GeV and $E_T^{\mathrm{jet2}} > 6.5$ GeV.

The variable x_γ^{OBS} is defined as

$$x_\gamma^{\mathrm{OBS}} = \frac{\sum_{\mathrm{jets}}(E^{\mathrm{jet}} - p_Z^{\mathrm{jet}})}{\sum_{\mathrm{hadrons}}(E - p_Z)} \;, \tag{1}$$

where E^{jet} and p_Z^{jet} are the energy and the longitudinal momentum of the jet. The upper sum runs over the two jets with highest transverse energy and the lower sum runs over all final state hadrons.

3 Data Selection and jet search

A three-level trigger was used to select events online [14]. The sample was separated offline into three subsamples corresponding to photoproduction ($Q^2 < 1.0$ GeV^2), Beam Pipe Calorimeter (BPC, $0.1 < Q^2 < 0.55$ GeV^2) and DIS ($1.5 < Q^2 < 2000$ GeV^2). The photoproduction sample was selected by demanding no scattered electron in the calorimeter. The BPC sample required a scattered positron in the BPC with $E_{\mathrm{e}} > 12.5$ GeV. DIS selection required a scattered positron in the CAL with $E_{\mathrm{e}} > 10.0$ GeV.

The sample was also required to have an event vertex consistent with the nominal interaction vertex, $|Z_{\mathrm{vtx}}| < 50.0$ cm, and to satisfy $0.2 < y_{\mathrm{JB}} < 0.55$. Jets were then reconstructed using the $kt-$cluster algorithm running over a combination of CAL and tracking information known as Energy Flow Objects [15] (EFOs). In all cases the EFOs were boosted into the photon-proton centre of mass frame prior to jet finding. At least two jets were required in each event within the pseudorapidity range $-3 < \eta^{\mathrm{jet}} < 0$ ordered according to decreasing E_T^{jet}. They were further required to satisfy $E_T^{\mathrm{jet1}} > 7.5$ GeV and $E_T^{\mathrm{jet2}} > 6.5$ GeV.

4 QCD calculations

4.1 NLO calculations

The NLO QCD calculations of jet production cross sections used in this analysis are based on the program DISASTER++ [16], in the case of DIS, and the calculation of Frixione and Ridolfi [17,18,19] (FR) in photoproduction. In both calculations, the number of flavours was set to five. The renormalisation and factorisation scales were set to $\mu^2 = \mu_R^2 = \mu_F^2 = Q^2 + (E_T^{\mathrm{jet}})^2$ or Q^2 in DIS and $\mu^2 = (E_T^{\mathrm{jet}})^2$ in photoproduction. In photoproduction and DIS the CTEQ5M1 sets were used for the proton PDFs, and in photoproduction the GRV [21] and AFG [20] parameterisations of the photon PDFs were used. Hadronisation corrections were applied to the parton level NLO cross section before comparisons to data were made.

4.2 Monte Carlo predictions

Predictions of Herwig 6.4 [22] using CTEQ5L for the proton PDFs and SaS2D for the photon PDFs were generated using parameters tuned [23] to many previous HERA and LEP measurements. In the SaS2D parameterisation the structure of the virtual photon is suppressed with increasing Q^2. Predictions were also generated with this suppression switched off. LO predictions are not shown here however a full discussion can be found in [11].

5 Results

Figure 1 shows the differential dijet cross section, $d\sigma/dQ^2$, compared to the next-to-leading order QCD predictions described in section 4.1. The cross section split in the direct-enhanced region ($x_\gamma^{\rm OBS} \geq 0.75$) and the resolved-enhanced region ($x_\gamma^{\rm OBS} < 0.75$) is also shown. The prediction of Disaster++ with $\mu^2 = Q^2 + (E_T^{\rm jet})^2$, describes the shape of the measured total dijet cross section but underestimates its magnitude by approximately 30%. The measured cross section for $x_\gamma^{\rm OBS} > 0.75$ is reasonably well described by the calculation for all Q^2. However, the prediction dramatically underestimates the measured cross section for $x_\gamma^{\rm OBS} < 0.75$. The photoproduction prediction of Frixione and Ridolfi describes all cross sections well.

Figure 2 shows the ratio, $R = \sigma(x_\gamma^{\rm OBS} < 0.75)/\sigma(x_\gamma^{\rm OBS} > 0.75)$ compared to the NLO predictions. The Q^2 dependence of the data is stronger at low $\overline{E}_T^2$ than at higher $\overline{E}_T^2$, showing that the low-$x_\gamma^{\rm OBS}$ component is suppressed at low Q^2 as $\overline{E}_T^2$ increases, and at low $\overline{E}_T^2$ as Q^2 increases. The photoproduction calculations using GRV are in reasonable agreement with the data, whereas those using AFG are below the data. In the DIS region, the predictions lie below the data at low $\overline{E}_T^2$. However, some suppression in the ratio as a function of Q^2 is observed.

Also studied were the double differential cross sections, $d^2\sigma/dQ^2dE_T^{\rm jet1}$, as a function of $E_T^{\rm jet1}$ and $d^2\sigma/dQ^2d\eta^F$ in different Q^2 ranges (not shown). In both cases the photoproduction NLO gave a good description of both cross sections. In DIS the NLO predictions describe the $d^2\sigma/dQ^2dE_T^{\rm jet1}$ cross sections for low and high $E_T^{\rm jet1}$ but lie below the data for middle $E_T^{\rm jet1}$. The DIS predictions also lie below the data in the forward regions ($\eta \to 0$) of the cross sections $d^2\sigma/dQ^2d\eta^F$, where the effects of photon structure are expected [11].

6 Summary and conclusions

Dijet differential cross sections have been measured in the range $0 < Q^2 < 2000$ GeV^2 with $0.2 < y < 0.55$, $-3 < \eta^{\rm jet} < 0$ and $E_T^{\rm jet1,jet2} > 7.5$ and 6.5 GeV, as a function of Q^2, $E_T^{\rm jet1}$ and η^F in the photon-proton centre-of-mass frame. These precise measurements, spanning a large range of photon virtualities, including photoproduction, DIS, and the transition region between them, are qualitatively described by leading-logarithmic parton-shower MC models which introduce virtual photon structure, suppressed with increasing Q^2. These data may constrain such parton densities significantly if used in future fits.

The currently available next-to-leading-order QCD calculations have large uncertainties at low Q^2, where the presence of a resolved-photon contribution may be expected. Improved higher-order or resummed calculations are needed. In DIS, the NLO QCD predictions generally underestimate the cross section at low-$x_\gamma^{\rm OBS}$ relative to that at high $x_\gamma^{\rm OBS}$.

References

1. PLUTO Coll. , C. Berger et al., Nucl. Phys. **B 281**, 365 (1987)
2. M. Krawczyk, A. Zembrzuski, M. Staszel (Warsaw U.), Phys. Rept. **345**, 265 (2001)
3. E.D. Bloom et al., Phys. Rev. Lett. **23**, 930 (1969)
4. M. Breidenbach et al., Phys. Rev. Lett. **23**, 935 (1969)
5. J.I. Friedman and H.W. Kendall, Annual Review of Nuclear Science **22**, 203 (1972)
6. H1 Coll. , C. Adloff et al., Eur. Phys. J. **C 13**, 397 (2000)
7. H1 Coll. , A. Aktas et al.. Hep-ex/0401010
8. ZEUS Coll. , J. Breitweg et al., Phys. Lett. **B 479**, 37 (2000)
9. ZEUS Coll., M. Derrick et al., Phys. Lett. **B 322**, 287 (1994)
10. ZEUS Coll., M. Derrick et al., Phys. Lett. **B 348**, 665 (1995)
11. ZEUS Coll., S. Chekanov et al., hep-ex/0404033
12. S. Catani et al., Nucl. Phys. **B 406**, 187 (1993)
13. S.D. Ellis and D.E. Soper, Phys. Rev. **D 48**, 3160 (1993)
14. ZEUS Coll., U. Holm (ed.), *The ZEUS Detector*. Status Report (unpublished), DESY (1993), available on `http://www-zeus.desy.de/bluebook/bluebook.html`
15. G.M. Briskin. Ph.D. Thesis, Tel Aviv University, 1998. (Unpublished)
16. D. Graudenz, Preprint hep-ph/9710244, 1997
17. S. Frixione, Z. Kunszt and A. Signer, Nucl. Phys. **B 467**, 399 (1996)
18. S. Frixione, Nucl. Phys. **B 507**, 295 (1997)
19. S. Frixione and G. Ridolfi, Nucl. Phys. **B 507**, 315 (1997)
20. P. Aurenche, J.P. Guillet and M. Fontannaz, Z. Phys. **C 64**, 621 (1994)
21. M. Gl*ü*ck, E. Reya and A. Vogt, Phys. Rev. **D 46**, 1973 (1992).
22. G. Corcella, I.G. Knowles, G. Marchesini, S. Moretti, K. Odagiri, P. Richardson, M.H. Seymour and B.R. Webber, JHEP **0101**, 010 (2001)
23. J.M. Butterworth and S. Butterworth, Comp. Phys. Comm. **153**, 164 (2003)

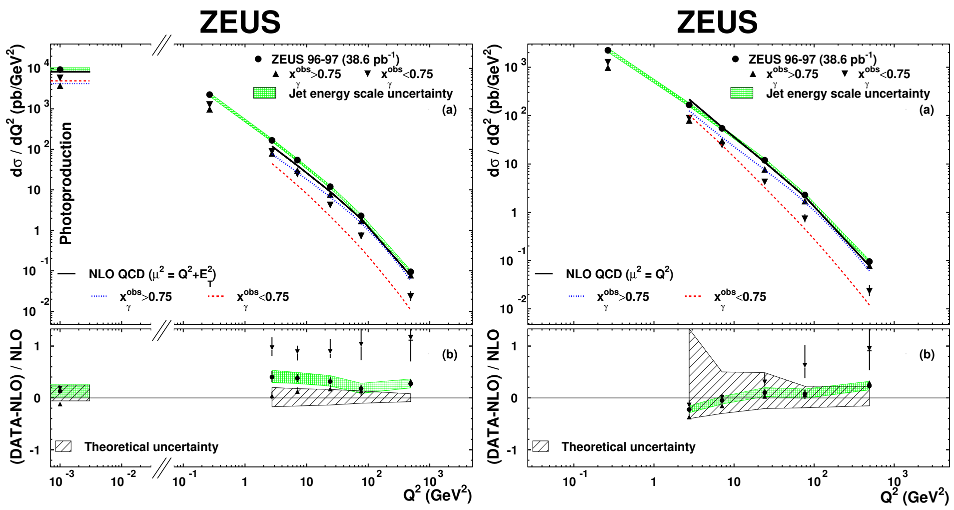

Figure 1. Measured dijet cross-sections $d\sigma/dQ^2$ for $x_\gamma^{\rm OBS} > 0.75$ (upwards triangles), for $x_\gamma^{\rm OBS} < 0.75$ (downwards triangles) and for the whole $x_\gamma^{\rm OBS}$ region (black dots), for dijet events, compared to NLO predictions.

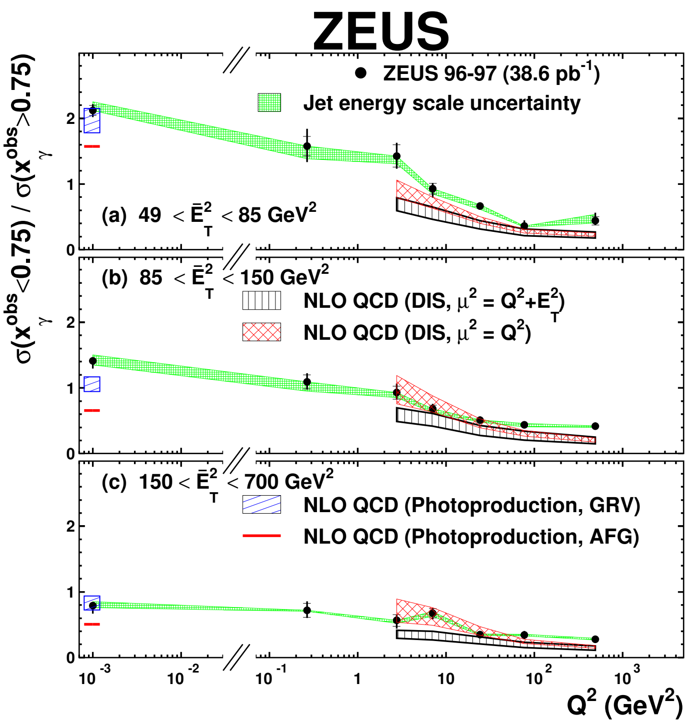

Figure 2. Measured ratio $R = \sigma(x_\gamma^{\rm OBS} < 0.75)/\sigma(x_\gamma^{\rm OBS} > 0.75)$ as a function of Q^2 in different regions of $\overline{E}_T^2$ (black dots). NLO QCD calculations predictions are also shown. The hatched bands represent the theoretical uncertainties.